



# Strong correlation of oxygen vacancies in bridgmanite with Mg/Si ratio

Zhaodong Liu<sup>a,b,\*</sup>, Tiziana Boffa Ballaran<sup>a</sup>, Rong Huang<sup>a</sup>, Daniel J. Frost<sup>a</sup>, Tomoo Katsura<sup>a,c</sup>

HPSTAR  
815-2019

<sup>a</sup> Bayerisches Geoinstitut, University of Bayreuth, 95440 Bayreuth, Germany

<sup>b</sup> State Key Laboratory of Superhard Materials, Jilin University, Changchun 130012, China

<sup>c</sup> Center for High Pressure Science and Technology Advanced Research, Beijing 100094, China

## ARTICLE INFO

### Article history:

Received 8 October 2018

Received in revised form 4 June 2019

Accepted 27 June 2019

Available online xxxx

Editor: B. Buffett

### Keywords:

oxygen vacancy

Mg/Si ratio

bridgmanite

volatile

slab stagnation

lower mantle

## ABSTRACT

The variation of an oxygen vacancy (OV) in the form of an  $\text{MgAlO}_{2.5}$  component in bridgmanite with Mg/Si ratios of bulk compositions was clarified using phase relations in the ternary system  $\text{MgO}-\text{AlO}_{1.5}-\text{SiO}_2$  at a pressure of 27 GPa and a temperature of 2000 K using advanced multi-anvil techniques. Both normal and reversed experiments suggest that significant amounts of the OV component exist in bridgmanite synthesized from bulk compositions with Mg/Si ratios above unity. The OV component significantly decreases with decreasing Mg/Si ratio, and it finally becomes negligible for Mg/Si ratios below unity. In contrast, the charge-coupled (CC) component of  $\text{AlAlO}_3$  becomes more dominant. The ternary phase relations further indicate that bridgmanite in a pyrolitic or peridotitic lower mantle will contain certain amounts of OV component, while that in mid-ocean ridge basalts (MORB) will not contain any amount of this component. Our study suggests that significant amounts of volatiles such as argon trapped by the OV of bridgmanite may be induced into the ambient lower mantle, while they cannot be brought into basaltic slabs by bridgmanite but other phases such as hydrous phases. The decrease of the OV in bridgmanite with decreasing Mg/Si ratio may offer a simple explanation for the occurrence of some stagnant slabs in the lower mantle.

© 2019 Elsevier B.V. All rights reserved.

## 1. Introduction

Bridgmanite, the most abundant phase in the lower mantle (about 80% by volume), can contain significant amounts of aluminum (Al) (Irifune, 1994; Tschauner et al., 2014). Al substitution in bridgmanite can occur in the forms of  $\text{AlAlO}_3$  and  $\text{MgAlO}_{2.5}$ . These two components, referred to as the CC (charge-couple) component and OV (oxygen-vacancy) component, respectively, affect differently the chemistry and elastic properties of bridgmanite. The OV component appears to considerably decrease the bulk modulus of bridgmanite (Zhang and Weidner, 1999; Brodholt, 2000; Daniel et al., 2001; Andraut et al., 2007) and it may transport water (Navrotsky, 1999; Murakami et al., 2002) and noble gases (Shcheka and Keppler, 2012) into the lower mantle (Liu et al., 2017a). In contrast, the CC component does not affect the bulk modulus significantly (Walter et al., 2004, 2006), and it cannot incorporate volatiles into the bridgmanite structure. Hence, it is important to investigate the conditions for which each Al substi-

tution mechanism dominates in order to understand the structure and geochemical circulation in the lower mantle.

In a pyrolitic mantle composition with an Mg/Si ratio of 1.3, bridgmanite coexists with ferropericlaite ( $\text{MgO}$ ) (Irifune, 1994), whereas it coexists with stishovite ( $\text{SiO}_2$ ) for the composition of mid-ocean ridge basalts (MORB) with a very low Mg/Si ratio of 0.5 (Hirose et al., 2005). It is expected that the OV component will dominate in bridgmanite for MgO-rich conditions rather than for  $\text{SiO}_2$ -rich conditions (Navrotsky, 1999; Walter et al., 2006; Andraut et al., 2007). Navrotsky et al. (2003), Kojitani et al. (2007) and Liu et al. (2017a) indeed showed that the OV component was prevalent in the system  $\text{MgSiO}_3-\text{MgAlO}_{2.5}$  that corresponded to MgO-rich conditions, at pressures corresponding to the uppermost part of the lower mantle. Petrological studies on the system  $\text{MgSiO}_3-\text{Al}_2\text{O}_3$  (Irifune et al., 1996; Kubo and Akaogi, 2000; Liu et al., 2016, 2017b), which provided more Si-rich conditions, suggested that the CC component becomes dominant in the deeper lower mantle, while the OV component becomes negligible. Furthermore, Walter et al. (2006) studied phase relations in  $\text{MgSiO}_3-\text{MgAlO}_{2.5}$ ,  $\text{MgSiO}_3-\text{MgAl}_2\text{O}_4$ , and  $\text{MgSiO}_3-\text{Al}_2\text{O}_3$  systems using a laser-heated diamond anvil cell (LHDAC) combined with *in-situ* X-ray diffraction, suggesting that the OV component plays a negligible role even in MgO-rich systems in the lower mantle.

\* Corresponding author at: Bayerisches Geoinstitut, University of Bayreuth, 95440 Bayreuth, Germany.

E-mail address: liu\_zhaodong@jlu.edu.cn (Z. Liu).

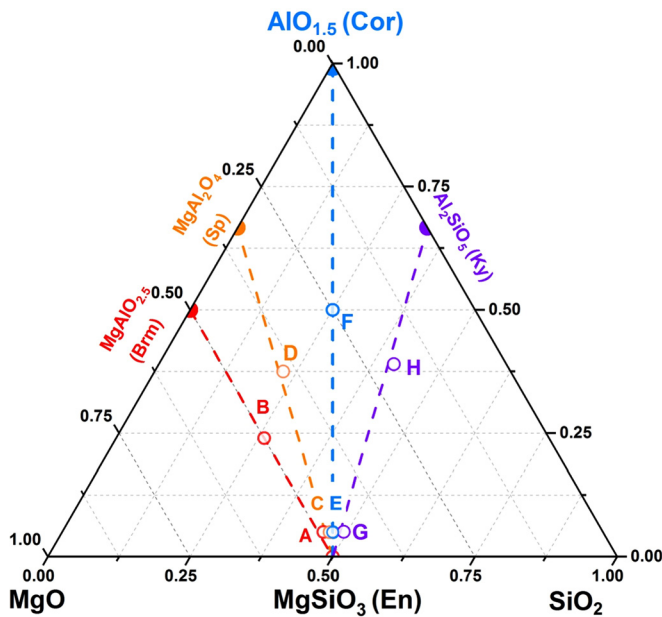


**Fig. 1.** Starting compositions in the system MgO–AlO<sub>1.5</sub>–SiO<sub>2</sub> (mol%) used in this study. Red circles of A and B represent starting compositions along the system MgSiO<sub>3</sub> (En)–MgAlO<sub>2.5</sub> (Brm); yellow symbols of C and D represent those along the system MgSiO<sub>3</sub>–MgAl<sub>2</sub>O<sub>4</sub> (Sp); blue symbols of E and F represent those along the system MgSiO<sub>3</sub>–AlO<sub>1.5</sub> (Cor), purple symbols of G and H represent those along the system MgSiO<sub>3</sub>–Al<sub>2</sub>SiO<sub>5</sub> (Ky). Abbreviation: En: MgSiO<sub>3</sub> enstatite, Brm: MgAlO<sub>2.5</sub> brownmillerite, Sp: MgAl<sub>2</sub>O<sub>4</sub> spinel, Cor: Al<sub>2</sub>O<sub>3</sub> corundum, Ky: Al<sub>2</sub>SiO<sub>5</sub> kyanite. (For interpretation of the colors in the figure(s), the reader is referred to the web version of this article.)

Thus, it is still unclear what effect the bulk composition has on the substitution mechanism of Al in bridgmanite.

In this study, we systematically investigated the content of the OV and CC component in bridgmanite with varying Mg/Si ratios for the bulk compositions in ternary system MgO–AlO<sub>1.5</sub>–SiO<sub>2</sub> using a multi-anvil press with tungsten carbide anvils. The pressure and temperature condition in this study were 27 GPa and 2000 K in order to avoid the presence of majorite, which may have cause additional complication in the phase relations. With these experiments, we could constrain the OV content in bridgmanite in the uppermost part of the lower mantle, and then discuss its implications for the mineralogy, dynamics, and geochemical cycling in the lower mantle.

## 2. Materials and methods

We prepared eight different starting compositions, which are shown in Fig. 1. The starting materials A, C, E, and G are glasses with compositions of En<sub>90</sub>Brm<sub>10</sub> (Brm: MgAlO<sub>2.5</sub> brownmillerite), En<sub>95</sub>Sp<sub>5</sub> (Sp: MgAl<sub>2</sub>O<sub>4</sub> spinel), En<sub>95</sub>Cor<sub>5</sub> (Cor: Al<sub>2</sub>O<sub>3</sub> corundum), and En<sub>95</sub>Ky<sub>5</sub> (Ky: Al<sub>2</sub>SiO<sub>5</sub> kyanite), while B, D, F, and H are fine-grained oxide mixtures of En<sub>52</sub>Brm<sub>48</sub>, En<sub>50</sub>Sp<sub>50</sub>, En<sub>50</sub>Cor<sub>50</sub>, and En<sub>50</sub>Ky<sub>50</sub>. Their general features are as follows. The compositions of A (Mg/Si = 1.06) and B (Mg/Si = 1.75) mixtures are on the tie line of MgSiO<sub>3</sub> to MgAlO<sub>2.5</sub>. The C (Mg/Si = 1.02) and D (Mg/Si = 1.76) mixtures are on the tie line of MgSiO<sub>3</sub> to MgAl<sub>2</sub>O<sub>4</sub>, those of mixtures E (Mg/Si = 1.00) and F (Mg/Si = 0.99) are on the tie line of MgSiO<sub>3</sub> to Al<sub>2</sub>O<sub>3</sub>. Finally, the G (Mg/Si = 0.92) and H (Mg/Si = 0.48) mixtures are on the tie line of MgSiO<sub>3</sub> to Al<sub>2</sub>SiO<sub>5</sub>. The glasses were prepared from oxide mixtures of reagent-grade MgO, SiO<sub>2</sub>, and Al<sub>2</sub>O<sub>3</sub>, which were fused at a temperature of 2000 K for 1 h, quenched into cold water and ground into fine-grained powder. This process was repeated three times in order to obtain homogeneous glass starting material. The fine-grained oxide mixtures were prepared from reagent-

grade oxide chemicals with very small grain sizes of ~100 nm in order to enhance reactions at 27 GPa and 2000 K (Liu et al., 2016, 2017b). The compositions of these starting materials were measured with an electron probe microanalyze (see Supplementary Table S1). The starting materials were put into platinum capsules, and heated at 800 K for 1 h before being used in the high-pressure cell assembly in order to minimize the amount of adhesive water.

Synthesis experiments at 27 GPa and 2000 K were performed using a Cr<sub>2</sub>O<sub>3</sub>-doped MgO octahedra with 7-mm edge length and a LaCrO<sub>3</sub> sleeve for heating in combination with tungsten carbide cubes with 3-mm truncated edge lengths in a Kawai-type multi-anvil apparatus with a press load of 15 MN at the Bayerisches Geoinstitut, University of Bayreuth (IRIS-15) (Ishii et al., 2016). Pressure calibrations at 2000 K were calibrated based on the solubility of Al<sub>2</sub>O<sub>3</sub> in bridgmanite coexisting with corundum (Liu et al., 2017b). The pressure uncertainties of these experiments are ±0.5 GPa.

Textural observations and chemical analyses of the recovered samples were performed using an LEO1530 scanning electron microscope (SEM) and a JEOL JXA-8200 electron probe microanalyzer (EPMA) operating at an acceleration voltage of 15 kV and a beam current of 5 nA with enstatite and forsterite for Mg and Si standards, respectively, and corundum for Al. We measured the composition of pure MgSiO<sub>3</sub> bridgmanite (Liu et al., 2016) using the same setting as a benchmark analysis. The phases present were identified using a micro-focused X-ray diffractometer (MF-XRD), a Bruker D8 DISCOVER equipped with a two-dimensional solid state detector (VANTEC500), and a micro-focus source (I $\mu$ S) with Co-K $\alpha$  radiation operated at 40 kV and 500  $\mu$ A. The X-ray beam was focused to 50  $\mu$ m using an IFG polycapillary X-ray mini-lens. XRD profiles of each sample were collected for two hours. The Bragg angles ( $2\theta$ ) of the MF-XRF were calibrated using MgSiO<sub>3</sub> bridgmanite as an external standard.

## 3. Results

### 3.1. Phase assemblages

Experimental conditions and phases present in the recovered samples are summarized in Table 1. The starting materials with compositions near pure-MgSiO<sub>3</sub> (A, C, and E) produce a single-phase of bridgmanite except for the SiO<sub>2</sub>-rich system (G), which crystallizes to a bridgmanite + stishovite assemblage from XRD and SEM observations (Figs. 2 and 3). The run products from starting materials with a larger secondary components (B, D, F, and H) consist of bridgmanite plus one or two additional phases (Figs. 2 and 3). The coexisting phases change from periclase + CF phase (B) to CF phase + corundum (D) to corundum (F) and finally to corundum + stishovite (G).

### 3.2. Composition

Compositions of bridgmanite in the recovered samples are shown in Table 2, and those of additional phases coexisting with bridgmanite are shown in Supplementary Table S2. Bridgmanite for A, C, E, and G contains almost the same Al<sub>2</sub>O<sub>3</sub> content (5 wt.%), which is also comparable with that of their glass starting material. The Mg/Si ratio of these synthesized bridgmanite is almost close to that of the bulk starting materials within analytical uncertainties except G. The Mg/Si ratio of bridgmanite from G is 0.99, which is significantly higher than that of the starting material (0.92) due to the existence of some amount of minor stishovite in this sample. The Al<sub>2</sub>O<sub>3</sub> content in bridgmanite increases from 8.1 wt.% for B to 10.5 wt.% for D and to 12.6 wt.% for F and then decrease to 10.9 wt.% for H. It's found that the appearing CF phase in B and D

**Table 1**  
Starting materials, experimental conditions, and runs products.

Let.	Start Comp.	Run No.	P (27 GPa)/T (2000 K)/t (h)	Phases
A	En <sub>90</sub> Brm <sub>10</sub>	IRIS423	5	Brg
B	En <sub>52</sub> Brm <sub>48</sub>	IRIS427	22	Brg + CF phase + Per
B <sup>a</sup>	En <sub>52</sub> Brm <sub>48</sub> <sup>a</sup>	IRIS478 <sup>b</sup>	20	Brg + CF phase + Per
C	En <sub>95</sub> Sp <sub>5</sub>	IRIS450	6	Brg
D	En <sub>50</sub> Sp <sub>50</sub>	IRIS446	26	Brg + CF phase + Cor
D <sup>a</sup>	En <sub>50</sub> Sp <sub>50</sub> <sup>a</sup>	IRIS478 <sup>b</sup>	20	Brg + CF phase + Cor
E	En <sub>95</sub> Cor <sub>5</sub>	IRIS423	Same with A	Brg
F	En <sub>50</sub> Cor <sub>50</sub>	IRIS427	Same with B	Brg + Cor
G	En <sub>95</sub> Ky <sub>5</sub>	IRIS450	Same with C	Brg + Sti
H	En <sub>50</sub> Ky <sub>50</sub>	IRIS446	Same with D	Brg + Sti + Cor

Abbreviations: Brg, bridgmanite; CF phase, calcium ferrite-type structure of MgAl<sub>2</sub>O<sub>4</sub>; Per, periclase; Cor, corundum; Sti, stishovite.

<sup>a</sup> Presents the starting material for B and D synthesized under 27 GPa and 2000 K for 22 h.

<sup>b</sup> Represents the reversed experiment.

contains significant amounts of the Mg<sub>2</sub>SiO<sub>4</sub> component, and this component would decrease from 34 mol% from B to 30 mol% for D. The corundum in samples D, F, and H contains 19, 21, and 20 mol% MgSiO<sub>3</sub> component, respectively. The periclase and stishovite in B and H, respectively, also contain small amounts of Al<sub>2</sub>O<sub>3</sub> component of 0.3 and 2.0 mol%. We also did one reversed experiment in the run IRIS478 for the powder sample of the run products of B and D, which were synthesized at 27 GPa and 2000 K for 22–26 h in the runs IRIS427 and IRIS446, for additional 20–26 h at the same pressure and temperature. Bridgmanite from B and D in this reversed run contains about 8.3 and 10.9 wt.% Al<sub>2</sub>O<sub>3</sub>, respectively, which are comparable to those (8.1 and 10.5 wt.%) for B and D in the synthesized runs IRIS427 and IRIS446. The CF phase, corundum, and periclase also show nearly consistent compositions with those in the above synthesis runs within analytical uncertainties. This fact suggests that chemical equilibrium was achieved for experiments at 27 GPa and 2000 K for keeping 22–26 h in our experiments.

The content of the OV (MgAlO<sub>2.5</sub>) and CC (AlAlO<sub>3</sub>) components in bridgmanite were derived from the reaction of Mg<sub>x</sub>Al<sub>2</sub>Si<sub>y</sub>O<sub>x+1.5z+2y</sub> = y MgSiO<sub>3</sub> + (x – y) MgAlO<sub>2.5</sub> + (z – x + y)/2 AlAlO<sub>3</sub> (x + y + z = 2, Liu et al., 2017a). Fig. 4a shows the variation of the OV and CC content in the synthesized bridgmanite with Al pfu (pfu: per formula units) of 0.1 as a function of the Mg/Si ratio. It was noted that the OV content in bridgmanite rapidly decreases from 4.9 mol% to approximately zero with the Mg/Si ratio decreasing from 1.05 for bridgmanite synthesized from A to 1.00 for that from G. In contrast, the corresponding CC content increases from 2.6 to 5.6 mol%. This fact suggests that both OV and CC mechanisms take place in the MgO-rich systems, with OV being dominant with respect to CC. However, with increasing Si content from A to G, the excess Si relative to Mg in the starting compositions favors the substitution of Al to form the CC component rather than the OV component. In addition, the OV and CC components suppress each other because the Al content in bridgmanite is nearly constant with changing Mg/Si ratio from A to G.

For bridgmanites with Al pfu above 0.1 that coexisted with one or two additional phases in B, D, F, and H, the OV gradually decreases from 2.0 mol% to nearly zero with a decreasing Mg/Si ratio from 1.02 to 1.00 for these synthesized bridgmanite (Fig. 4b). On the contrary, the CC content significantly increases with decreasing Mg/Si ratio in these bridgmanites. However, the slope of the dependence of the OV decreasing versus Mg/Si ratios for Al-rich bridgmanite is slightly lower than that for bridgmanite with Al pfu of 0.1, suggesting that the high Al might disfavor OV in Al-rich bridgmanite. These results can be explained by the decomposition of the MgAlO<sub>2.5</sub> and MgAl<sub>2</sub>O<sub>4</sub> component in the latter discussion.

### 3.3. Molar volume

The unit-cell lattice parameters of all phases present in the recovered samples are shown in Supplementary Table S3, and the molar volume of bridgmanite with Al pfu of 0.1 is plotted versus the Mg/Si ratio of the synthesized bridgmanite from different starting materials in Fig. 5a. In general, the molar volume of bridgmanite decreases with decreasing Mg/Si ratios. In more detail, the molar volume (24.59 cm<sup>3</sup>/mol) of bridgmanite synthesized in the En-Brm system, namely Mg-rich systems is significantly higher than those (24.50 cm<sup>3</sup>/mol) of bridgmanite crystallized in the more Si-rich systems such as En-Cor and En-Ky systems. In Fig. 5b, a linear function was used to fit the data for CC-bearing bridgmanite synthesized from the En-Cor and En-Ky systems by fixing the endmember of MgSiO<sub>3</sub> bridgmanite. The following equation was obtained:  $V(X) = 24.44 + 0.0135(5) \cdot X_{\text{AlAlO}_3}$  ( $0 < X_{\text{AlAlO}_3} \leq 15$ ), where  $V$  is the molar volume,  $X_{\text{AlAlO}_3}$  is the mole content of AlAlO<sub>3</sub> in bridgmanite, and the number in parentheses represents the standard deviation for the last digits. After that, we fitted the pure OV-bearing bridgmanite by subtracting the effect of the CC component and got  $V(X) = 24.44 + 0.023(2) \cdot X_{\text{MgAlO}_{2.5}}$  ( $0 < X_{\text{MgAlO}_{2.5}} < 6$ ), where  $X_{\text{MgAlO}_{2.5}}$  is the mole content of MgAlO<sub>2.5</sub> in bridgmanite. This fact suggests that 1 mol% OV would increase by 2 times higher for molar volume than the same content of CC component.

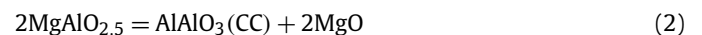
## 4. Discussions

### 4.1. Al substitution reactions in bridgmanite in the ternary system MgO–AlO<sub>1.5</sub>–SiO<sub>2</sub>

The compositions of bridgmanite, CF phase, periclase, corundum, and stishovite obtained in the present study are summarized in the phase diagram in the ternary system MgO–AlO<sub>1.5</sub>–SiO<sub>2</sub> (Fig. 6a). In the En-Brm system, the majority of the Brm component in the starting material A (En<sub>90</sub>Brm<sub>10</sub>) forms the OV component in bridgmanite, which can be explained by the following equation:



Since a small amount of the CC component is also contained in this bridgmanite, the following reaction should have occurred:



The starting material B (En<sub>52</sub>Brm<sub>48</sub>) produced periclase and a calcium-ferrite type (Mg, Al, Si)<sub>3</sub>O<sub>4</sub> (CF) in addition to bridgmanite



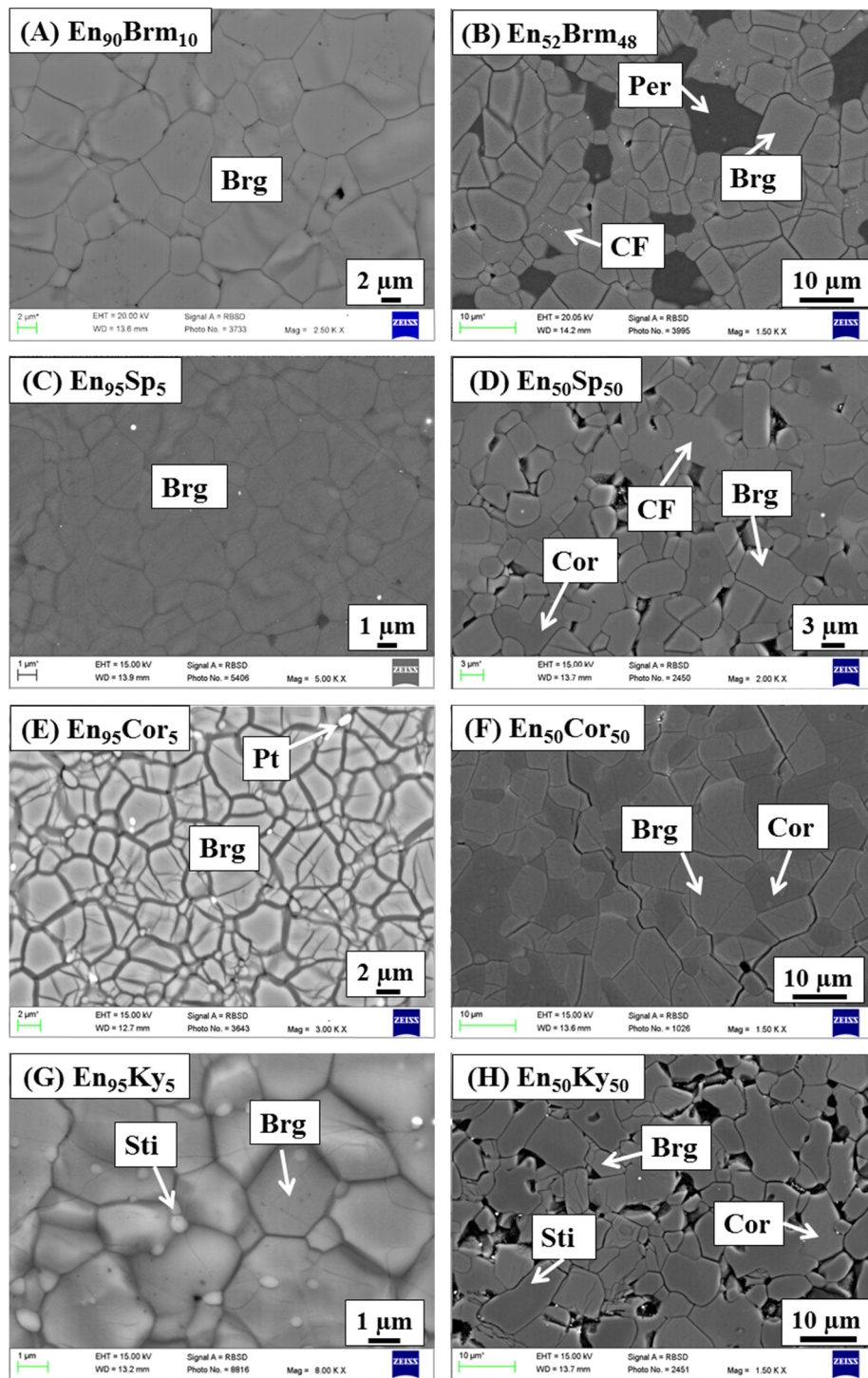
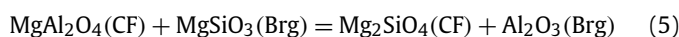


**Fig. 3.** BSE images of run products from various starting materials. Abbreviations: Brg, bridgmanite; Cor, corundum; CF, calcium ferrite-type structure of  $\text{MgAl}_2\text{O}_4$ ; Per, Periclase; Sti, stishovite; Pt, platinum.

plained by the following reaction:



It would thus result a wide solid solution for the CF phase between the endmembers of  $\text{MgAl}_2\text{O}_4$  and  $\text{Mg}_2\text{SiO}_4$ .

For the case of the En-Cor system, the starting material E ( $\text{En}_{95}\text{Cor}_5$ ) crystallized into a single phase of bridgmanite, whereas F ( $\text{En}_{50}\text{Cor}_{50}$ ) gave rise to bridgmanite with 11.7 mol% corundum, which is in agreement with previous studies (Irifune et al., 1996; Kubo and Akaogi, 2000; Liu et al., 2016, 2017b). In the En-Ky sys-

tem, the starting materials G ( $\text{En}_{95}\text{Ky}_5$ ) and H ( $\text{En}_{50}\text{Ky}_{50}$ ) crystallized to bridgmanite plus stishovite both without and with corundum (Fig. 2 and 3), respectively.

Noted that a single-phase region of bridgmanite was formed towards the MgO-rich region in the ternary phase relations (Fig. 6a). From the magnified ternary phase diagram in Fig. 6b, it can be seen that the compositions of bridgmanite with a low Al content (Al pfu of 0.1) synthesized in the En-Brm system ( $\text{Mg}/\text{Si} > 1$ ) are close to the ideal line of a complete oxygen vacancy substitution (OVS), while those obtained in the En-Cor and En-Ky

**Table 2**  
Chemical compositions of the synthesized bridgmanite.

Let.	Phases	MgO	Al <sub>2</sub> O <sub>3</sub>	SiO <sub>2</sub>	Total	Mg	Al	Si	O	Mg/Si	OV (mol.%)	CC (mol.%)
A	Brg (n = 18)	39.17 (43)	5.12 (33)	55.47 (77)	99.77 (76)	0.974 (7)	0.100 (7)	0.926 (6)	2.976 (4)	1.05 (2)	4.9 (13)	2.6 (3)
C	Brg (n = 48)	39.21 (48)	5.04 (19)	57.21 (75)	101.46 (92)	0.962 (9)	0.098 (4)	0.941 (5)	2.990 (5)	1.02 (2)	2.1 (13)	3.8 (4)
E	Brg (n = 26)	37.93 (22)	5.11 (12)	56.31 (30)	99.35 (55)	0.952 (5)	0.101 (2)	0.948 (4)	2.998 (3)	1.00 (1)	0.4 (8)	4.9 (3)
G	Brg (n = 30)	38.43 (55)	5.09 (18)	57.87 (55)	101.39 (66)	0.945 (10)	0.099 (4)	0.955 (6)	3.005 (6)	0.99 (2)	-1.0 (15)	5.5 (8)
B	Brg (n = 15)	37.34 (51)	8.09 (36)	54.48 (56)	99.90 (88)	0.930 (8)	0.159 (6)	0.910 (5)	2.989 (5)	1.02 (2)	2.0 (13)	7.0 (4)
B*	Brg (n = 25)	37.76 (53)	8.31 (35)	54.79 (46)	100.87(75)	0.931 (9)	0.162 (6)	0.906 (7)	2.988 (5)	1.03 (2)	2.5 (15)	6.9 (8)
D	Brg (n = 23)	37.00 (46)	10.52 (31)	54.39 (49)	101.92 (69)	0.904 (7)	0.203 (6)	0.891 (4)	2.992 (5)	1.02 (1)	1.3 (8)	9.5 (6)
D*	Brg (n = 16)	36.53 (44)	10.95 (42)	53.83 (61)	101.18 (89)	0.899 (6)	0.213 (8)	0.889 (7)	2.995 (4)	1.01 (1)	1.0 (10)	10.1 (5)
F	Brg (n = 15)	35.50 (52)	12.56 (31)	52.77 (32)	101.02 (98)	0.878 (7)	0.246 (6)	0.876 (4)	2.999 (5)	1.00 (1)	0.2 (9)	12.2 (7)
H	Brg (n = 14)	36.58 (48)	10.85 (53)	54.72 (37)	102.15 (60)	0.893 (10)	0.209 (9)	0.896 (6)	3.000 (5)	1.00 (2)	0 (1)	10.6 (4)

Oxide analyses are reported in wt.%. n: number of analysis points. The total cation number is normalized to two. Number in parentheses represents the standard deviation for the last digit (s). Abbreviations: Brg, bridgmanite; OV, MgAlO<sub>2.5</sub>; CC, AlAlO<sub>3</sub>.

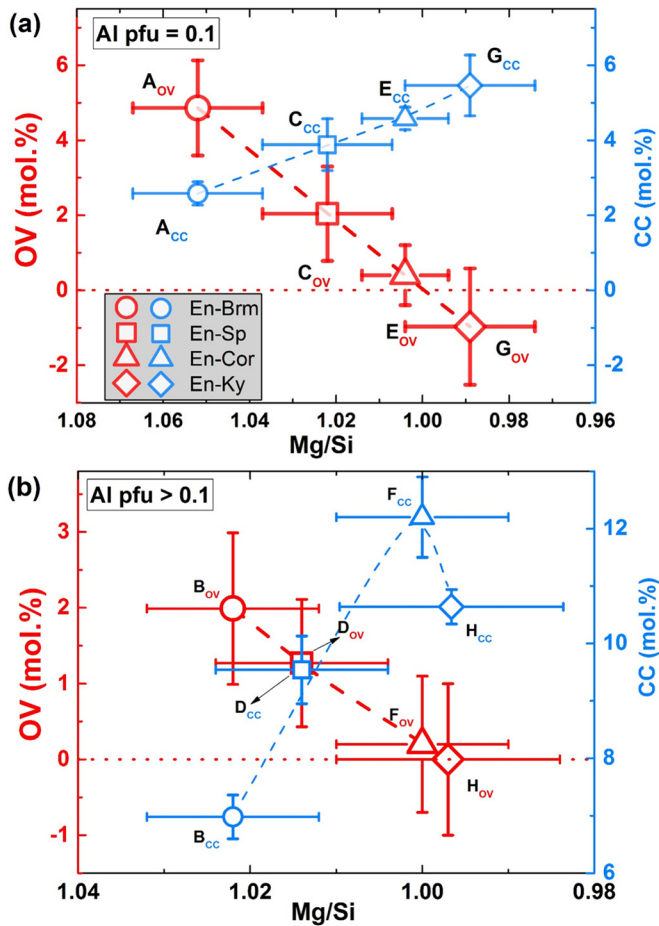


**Fig. 4.** Plots of the OV and CC components in bridgmanite with (a) Al pfu = 0.1 and (b) Al pfu > 0.1 as a function of their Mg/Si ratio. Red and blue dashed lines represent the variation of the OV and CC component, respectively. The red dotted line represents zero value of the OV content.

systems ( $Mg/Si \leq 1$ ) lie on the line of the charge-coupled substitution (CCS). This fact further supports the result obtained in Fig. 4a which demonstrates the excess MgO favors the OV component in bridgmanite, while the excess SiO<sub>2</sub> minimizes this component and favors the CC component.

Although Navrotsky et al. (2003) attempted to characterize the relations of the OV and CC content with bulk composition, they were not able to find any clear correlation. One possible reason is that in the mentioned study, the LH-DAC was the technique used for the majority of the high-pressure-temperature bridgmanite synthesis. However, to constrain the effect of the bulk composition on the Al substitution mechanism in bridgmanite, very

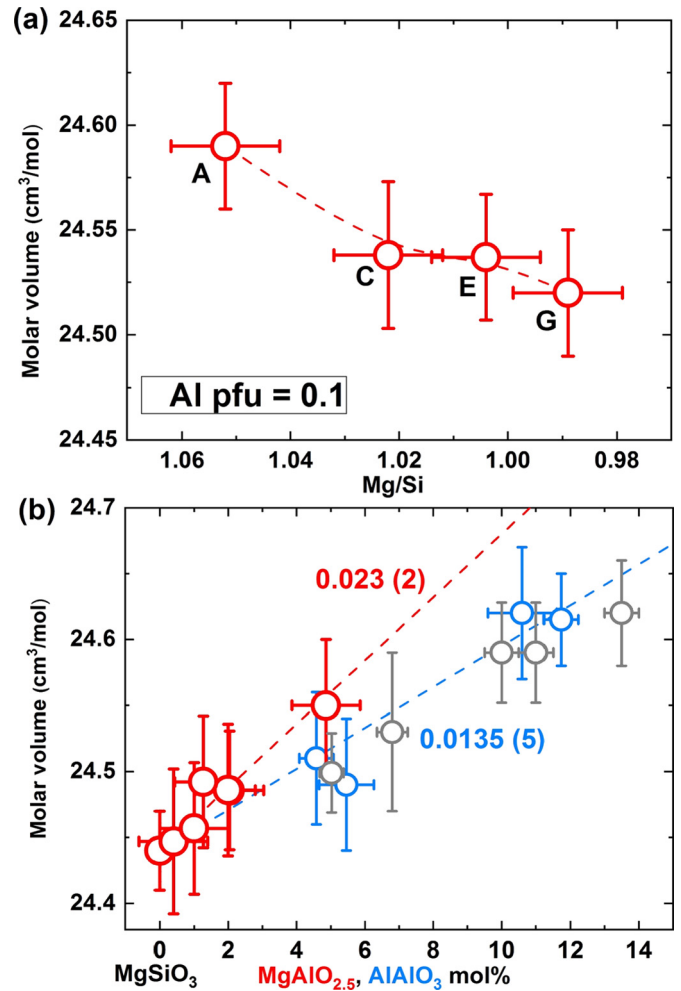


**Fig. 5.** (a) Molar volume of bridgmanite with Al pfu of 0.1 versus Mg/Si ratios. (b) Molar volume of bridgmanite versus the MgAlO<sub>2.5</sub> (OV) / AlAlO<sub>3</sub> (CC) content. Red and blue lines in (b), respectively, represent the linear fitting of the data in the systems MgSiO<sub>3</sub>-MgAlO<sub>2.5</sub> and MgSiO<sub>3</sub>-Al<sub>2</sub>O<sub>3</sub> in the present study. Black symbols are from Liu et al. (2017b). The red and blue digital data in (b), respectively, are the slope of molar volume versus the OV and CC component and the number in parentheses represents the error for the last digit.

reproducible pressure and temperature conditions, as well as high-quality chemical analysis by means of EPMA are required. These are very difficult conditions to obtain in LH-DAC experiments, though. Another reason may be that the majority of bridgmanite synthesized by means of multi-anvil runs in the mentioned study of Navrotsky et al. (2003) did not coexist with any excess phase and only a few of them coexisted with only one phase. Since the

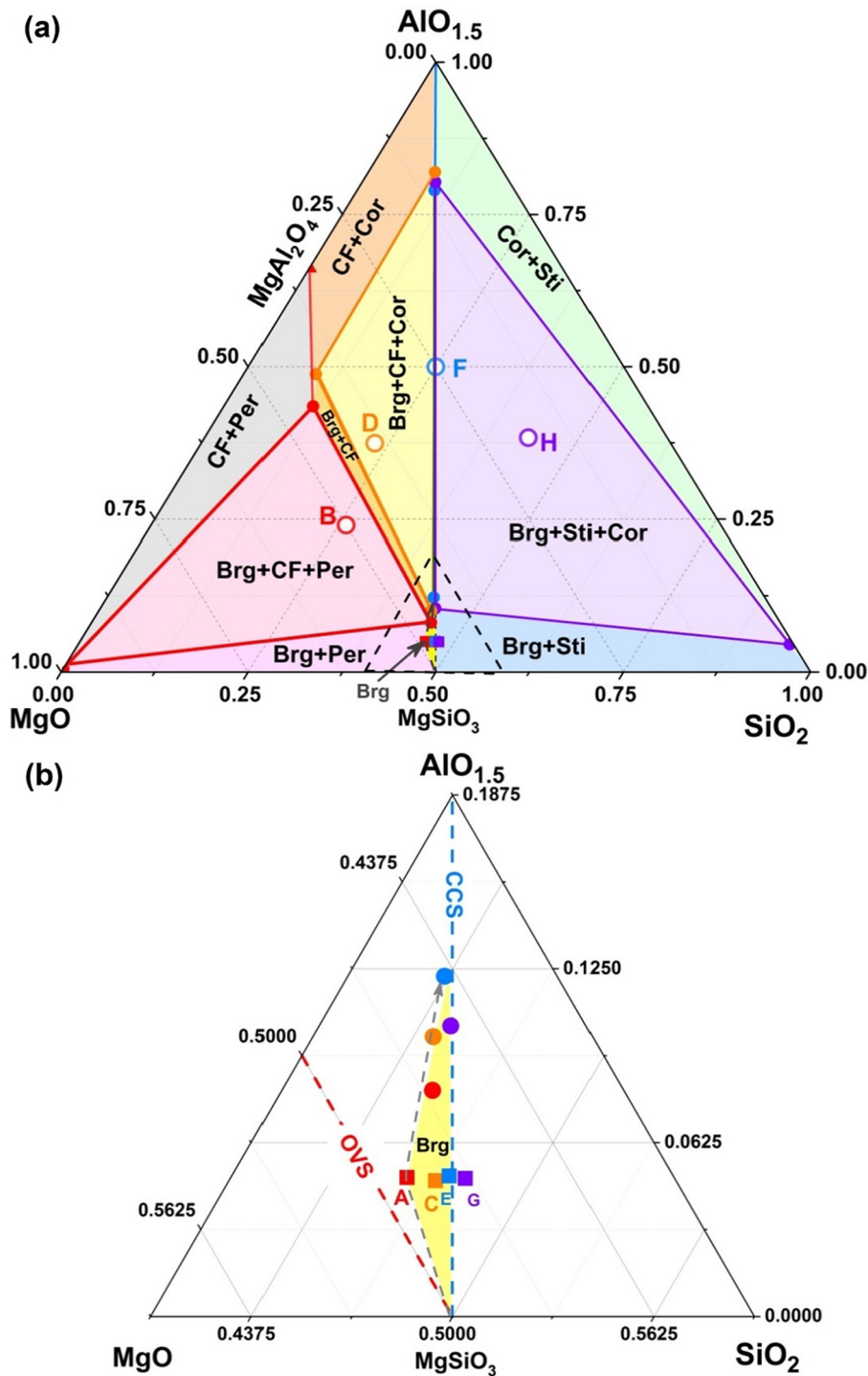


**Fig. 6.** (a) Ternary phase relations in the system MgO–AlO<sub>1.5</sub>–SiO<sub>2</sub> (mol%) at 27 GPa and 2000 K. (b) The magnified ternary phase relations from (a) marked by the dashed lines. Open symbols represent the starting compositions of B, D, F, and H, while solid circles are the compositions of the corresponding phases. Square solid symbols are the single bridgmanite phase synthesized from A, C, E, and G starting compositions. Abbreviations: Brg, bridgmanite; Cor, corundum; Per, periclase; CF, calcium ferrite-type structure of MgAl<sub>2</sub>O<sub>4</sub>; Sti, stishovite; CCS: charge-coupled substitution; OVS: oxygen vacancy substitution.

present chemical system consists of three components, i.e. MgO, Al<sub>2</sub>O<sub>3</sub>, and SiO<sub>2</sub>, two excess phases are necessary to fix the composition of bridgmanite. In our study, we conducted experiments both with and without excess phases for four different secondary components. This strategy allowed us to constrain the OV and CC contents as a function of the Mg/Si ratio.

Our result may explain the large variation of the bulk moduli found in aluminous bridgmanite from various starting mate-

rials and different Mg/Si ratios by Andraut et al. (2007). They found that bridgmanite from MgO-excess starting material possesses a relatively lower bulk modulus (243 GPa) than that from SiO<sub>2</sub>-excess starting material (272 GPa) under almost the same pressure range. This can be understood from the fact that OV-bearing bridgmanite becomes more compressible due to a higher molar volume of the OV component than the CC component (Fig. 5).

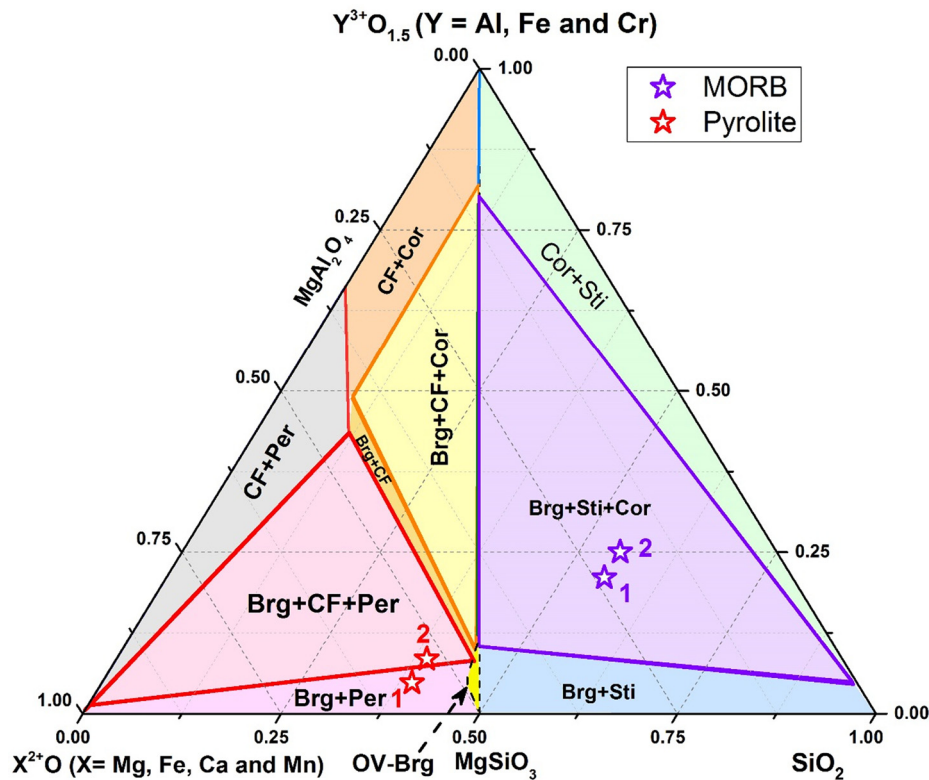


**Fig. 7.** Phase relations in the ternary system  $X^{2+}O$  ( $X = Mg, Fe, Ca, \text{ and } Mn$ )– $Y^{3+}O_{1.5}$  ( $Y = Al, Fe, \text{ and } Cr$ )– $SiO_2$  (mol%) for the upper part of the lower mantle. The blue and purple stars, respectively, represent the compositions of the pyrolite and MORB models for the case 1 and 2. The case 1 is that  $Fe^{3+}/\Sigma Fe$  in the lower mantle is identical to that (3%) in the upper mantle. The case 2 is that the  $Fe^{3+}/\Sigma Fe$  ratio of bridgmanite in equilibrium with metallic Fe is more than 50% for a typical mantle  $Al_2O_3$  content. Abbreviations: Brg, bridgmanite; Cor, corundum; Per, periclase; CF, calcium ferrite-type structure of  $MgAl_2O_4$ ; Sti, stishovite.

#### 4.2. Implications for geochemical circulation

Here, we investigated which Al substitution mechanism dominates in the lower-mantle rocks. We simplified the bulk composition of pyrolite and MORB by assuming that  $Fe^{2+}$ ,  $Ca^{2+}$  and  $Mn^{2+}$  behave in the same way as  $Mg^{2+}$ , denoted as  $X^{2+}$  hereafter, and that  $Fe^{3+}$  and  $Cr^{3+}$  behave in the same way as  $Al^{3+}$ , denoted as  $Y^{3+}$ . There are some debates about the  $Fe^{3+}$  fraction of the total iron ( $Fe^{3+}/\Sigma Fe$ ) in the lower mantle (Frost and McCammon, 2008) and the  $Fe^{3+}$  sites in bridgmanite depending on the trivalent cation content and pressure (Frost and Langenhorst, 2002; Fujino et al., 2012). We considered two extreme cases. The first case (case 1) is that  $Fe^{3+}/\Sigma Fe$  in the lower mantle is identical to that (3%) in the upper mantle (Frost and McCammon, 2008). The second case (case 2) is that the  $Fe^{3+}/\Sigma Fe$  ratio of bridgmanite in equilibrium with metallic Fe is more than 50% for a typical mantle  $Al_2O_3$  content (e.g., McCammon, 1997; Frost et al., 2004; Frost and McCammon, 2008) and  $Fe^{3+}$  prefers Mg sites due to the similar cation size in the uppermost lower mantle (Fujino et al., 2012). In the case 1, the bulk X:Y:Si ratios of pyrolite and MORB are 0.57:0.05:0.38 and 0.34:0.18:0.48, respectively. In the case 2, the bulk X:Y:Si ratios of pyrolite and MORB are 0.54:0.08:0.38 and 0.31:0.21:0.48, respectively. As shown in Fig. 7, the pyrolite compositions for the case 1 and 2 are located in the region of bridgmanite + periclase and that of bridgmanite + CF phase + periclase, respectively. Therefore, the OV component will be the major component of Al incorporation. We estimated that the bridgmanite from the pyrolite bulk composition will contain 9 and 4 mol% of the OV ( $XYO_{2.5}$ ) components in the case 1 and 2, respectively. In contrast, the bulk compositions of the MORB for both case 1 and 2 are located in the region of bridgmanite + stishovite + corundum, and bridgmanite cannot contain the OV component (Fig. 7). In more realistic estimations, the phases coexisting with bridgmanite in

the MORB compositions will not be stishovite + corundum but stishovite + NAL-phase. Nevertheless, bridgmanite in the MORB compositions will virtually contain no OV component.

The OV component in bridgmanite may transport some volatiles such as water (Navrotsky, 1999; Murakami et al., 2002) and noble gases (Shcheka and Keppler, 2012) into the lower mantle. If this assumption is correct, the present OV content in a pyrolite composition leads to a maximum water content of 1 wt% and significant noble gases such as argon and krypton above 1 wt% in bridgmanite in the ambient mantle. This is enough to explain the current experimental results of 1000 to 2000 ppm of water incorporation in Al-bearing bridgmanite in a peridotite composition (Murakami et al., 2002; Litasov et al., 2003). However, Bolfan-Casanova et al. (2000 and 2003), Litasov et al. (2003), and Panero et al. (2015) reported that Al-Fe-bearing bridgmanite could contain very limited amounts of water (10–400 ppm). These observations could be explained by the fact that Al and  $Fe^{3+}$  form the  $FeAlO_3$  component in bridgmanite, which may diminish the OV component. Bridgmanite in the MORB composition does not incorporate water as evidenced by Litasov et al. (2003) and volatiles because of no OV component. Thus, subducted MORB slabs will transport water and noble gases into the deep lower mantle by other hydrous phase such as aluminous stishovite (e.g., Pawley et al., 1993; Panero et al., 2003) and phase D (Pamato et al., 2015). The effects of iron on the substitution mechanisms of trivalent cation in bridgmanite must be studied in detail to understand the geochemical circulation between the surface and the deep mantle.

#### 4.3. Implications for slab stagnation in the lower mantle

Seismic tomography studies have observed some stagnant slabs at 600–1000 km depths in the lower mantle (e.g., Fukao and Obayashi, 2013). Since bridgmanite is the major mineral in this

region, its rheological properties can thus help understand these seismically observed slab stagnations (e.g., Boioli et al., 2017; Girard et al., 2016). The decreasing of OV will slow down the oxygen diffusivity in bridgmanite and thus cause an increase of its viscosity. The MORB slab, one of the most straightforward candidates, is thus more viscous than pyrolite in the lower mantle because the OV in bridgmanite in the former is significantly lower than the latter. More recently, a geodynamic model by Ballmer et al. (2017) found that bridgmanite in low-Mg/Si domains would enhance viscous entrainment in the lower mantle compared with high-Mg/Si regions, which may explain some stagnant slabs at ~1000 km depth. Our results demonstrated here indicate that bridgmanite in low-Mg/Si domains would have a higher viscosity than that in high-Mg/Si region due to an increase of the OV in bridgmanite with Mg/Si ratios, providing more evidences for their results. Therefore, the chemistry defect of bridgmanite with Mg/Si ratios may offer a simply explanation for some stagnant slabs in the lower mantle.

## 5. Conclusions

We studied the effect of Mg/Si ratios of the bulk compositions on the  $\text{MgAlO}_{2.5}$  (OV) and  $\text{AlAlO}_3$  (CC) content in bridgmanite in the ternary system  $\text{MgO-AlO}_{1.5}\text{-SiO}_2$  at a pressure of 27 GPa and a temperature of 2000 K. The OV content in bridgmanite, especially for a pyrolytic Al content, significantly decreases from 5 mol% to below zero with decreasing Mg/Si ratio from 1.05 to 0.99, while the CC content increases. The ternary phase relations suggest that periclase would maximize the OV component in bridgmanite, while stishovite would minimize this component and favor the CC component. The pyrolytic or peridotitic lower mantle is located in the region of bridgmanite + periclase or bridgmanite + periclase + CF phase and thereby have significant OV components in bridgmanite. In contrast, the MORB composition located in the region of bridgmanite + stishovite + corundum will contain virtually no OV in bridgmanite.

The presence of the OV component would cause a higher molar volume than that of the CC component for bridgmanite. The variation of the OV and CC components in bridgmanite with bulk Mg/Si ratios thus may explain the low and high value of the bulk modulus for bridgmanite under MgO-rich and  $\text{SiO}_2$ -rich conditions, respectively, in previous studies.

The uppermost region of the ambient lower mantle may be a chemical reservoir of volatiles such as water and argon due to the significant amounts of OV in bridgmanite. However, the presence of Fe, for which bridgmanite favors the  $\text{FeAlO}_3$  component, may decrease the OV component and reduce these volatiles storages. These volatile components cannot be transported into the basaltic slabs by bridgmanite in the lower mantle due to a negligible amount of oxygen vacancies in low Mg/Si regions. The chemistry defect of bridgmanite with Mg/Si ratio may thus help explain some stagnant slabs in the lower mantle.

## Acknowledgements

The authors thank D. Krauß and D. Wiesner for their technical supports in microprobe analyses, and E. Posner, H. Schulze, R. Njul, H. Fischer and S. Übelhack for their assistance with the cell assembly preparation. We also thank for the editor Bruce Buffett for processing our manuscript and anonymous reviewers for constructive comments. This project was financially supported by the Bayerisches Geoinstitut Visitor's Program and the Fundamental Research Funds for the Central Universities of Ministry of Education of China (Grant No. 45119031C037) for Z.L. This study is also supported by research grants to T.K. (BMBF: 05K13WC2, 05K16WC2; DFG: KA3434/3-1, KA3434/7-1, KA3434/8-1, KA3434/9-1). This

project has received funding from the European Research Council (ERC) under the European Union's Horizon 2020 research and innovation programme (Proposal No. 787 527).

## Appendix A. Supplementary material

Supplementary material related to this article can be found online at <https://doi.org/10.1016/j.epsl.2019.06.037>.

## References

- Andraut, D., Bolfan-Casanova, N., Bouhifd, M.A., Guignot, N., Kawamoto, T., 2007. The role of Al-defects on the equation of state of Al-(Mg,Fe)SiO<sub>3</sub> perovskite. *Earth Planet. Sci. Lett.* 263, 167–179.
- Ballmer, M.D., Houser, C., Hernlund, J.W., Wentzcovitch, R.M., Hirose, K., 2017. Persistence of strong silica-enriched domains in the Earth's lower mantle. *Nat. Geosci.* 10 (3), 236–240.
- Boioli, F., Carrez, P., Cordier, P., Devincere, B., Gouriet, K., Hirel, P., Ritterbex, S., 2017. Pure climb creep mechanism drives flow in Earth's lower mantle. *Sci. Adv.* 3 (3).
- Brodholt, J.P., 2000. Pressure-induced changes in the compression mechanism of aluminous perovskite in the Earth's mantle. *Nature* 407, 620–622.
- Bolfan-Casanova, N., Keppler, H., Rubie, D.C., 2000. Water partitioning between nominally anhydrous minerals in MgO-SiO<sub>2</sub>-H<sub>2</sub>O system up to 24 GPa: implications for the distribution of water in the Earth's mantle. *Earth Planet. Sci. Lett.* 182, 209–221.
- Bolfan-Casanova, N., Keppler, H., Rubie, D.C., 2003. Water partitioning at 660 km depth and evidence for very low water solubility in magnesium silicate perovskite. *Geophys. Res. Lett.* 30, 1905.
- Daniel, I.H., Cardon, H., Fiquet, G., Guyot, F., Mezouar, M., 2001. Equation of state of Al-bearing perovskite to lower mantle conditions. *Geophys. Res. Lett.* 28, 3789–3792.
- Frost, D.J., Langenhorst, F., 2002. The effect of AlO<sub>1.5</sub> on Fe-Mg partitioning between magnesiowüstite and magnesium silicate perovskite. *Earth Planet. Sci. Lett.* 199, 227–241.
- Frost, D.J., Liebske, C., Langenhorst, F., McCammon, C.A., Trønnes, R.G., et al., 2004. Experimental evidence for the existence of iron-rich metal in the Earth's lower mantle. *Nature* 248, 409–412.
- Frost, D.J., McCammon, C.A., 2008. The redox state of Earth's mantle. *Annu. Rev. Earth Planet. Sci.* 36, 389–420.
- Fujino, K., et al., 2012. Spin transition of ferric iron in Al-bearing Mg-perovskite up to 200 GPa and its implication for the lower mantle. *Earth Planet. Sci. Lett.* 317–318, 407–412.
- Fukao, Y., Obayashi, M., 2013. Subducted slabs stagnant above, penetrating through, and trapped below the 660 km discontinuity. *J. Geophys. Res.* 118, 2013JB010466.
- Girard, J., Amulele, G., Farla, R., Mohiuddin, A., Karato, S.-I., 2016. Shear deformation of bridgmanite and magnesiowüstite aggregates at lower mantle conditions. *Science* 351, 144–147.
- Hirose, K., Takafuji, N., Sata, N., Ohishi, Y., 2005. Phase transition and density of subducted MORB crust in the lower mantle. *Earth Planet. Sci. Lett.* 237, 239–251.
- Litasov, K., Ohtani, E., Langenhorst, F., Yurimoto, H., Kubo, T., Kondo, T., 2003. Water solubility in Mg-perovskites and water storage capacity in the lower mantle. *Earth Planet. Sci. Lett.* 211 (1), 189–203.
- Irifune, T., 1994. Absence of an aluminous phase in the upper part of the Earth's lower mantle. *Nature* 370, 131–133.
- Irifune, T., Koizumi, T., Ando, J., 1996. An experimental study of the garnet-perovskite transformation in the system MgSiO<sub>3</sub>-Mg<sub>3</sub>Al<sub>2</sub>Si<sub>3</sub>O<sub>12</sub>. *Phys. Earth Planet. Inter.* 96, 147–157.
- Ishii, T., Shi, L., Huang, R., Tsujino, N., Druzhbin, D., Myhill, R., Li, Y., Wang, L., Yamamoto, T., Miyajima, N., Kawazoe, T., Nishiyama, N., Higo, Y., Tange, Y., Katsura, T., 2016. Generation of pressure over 40 GPa using Kawai-type multi-anvil press with tungsten carbide anvils. *Rev. Sci. Instrum.* 87, 024501.
- Kojitani, H., Katsura, T., Akaogi, M., 2007. Aluminum substitution mechanisms in perovskite-type MgSiO<sub>3</sub>: an investigation by Rietveld analysis. *Phys. Chem. Miner.* 34, 257–267.
- Kubo, A., Akaogi, M., 2000. Post-garnet transitions in the system Mg<sub>4</sub>Si<sub>4</sub>O<sub>12</sub>-Mg<sub>3</sub>Al<sub>2</sub>Si<sub>3</sub>O<sub>12</sub> up to 28 GPa: phase relations of garnet, ilmenite and perovskite. *Phys. Earth Planet. Inter.* 121, 85–102.
- Liu, Z.D., Irifune, T., Nishi, M., Tange, Y., Arimoto, T., Shinmei, T., 2016. Phase relations in the system MgSiO<sub>3</sub>-Al<sub>2</sub>O<sub>3</sub> up to 52 GPa and 2000 K. *Phys. Earth Planet. Inter.* 257, 18–27.
- Liu, Z.D., Ishii, T., Katsura, T., 2017a. Rapid decrease of MgAlO<sub>2.5</sub> component in bridgmanite with pressure. *Geochem. Perspect. Lett.* 5, 12–18.
- Liu, Z.D., Nishi, M., Ishii, T., Fei, H.Z., Miyajima, N., Boffa Ballaran, T., Ohfujii, H., Sakai, T., Wang, L., Shcheka, S., Arimoto, T., Tange, Y., Higo, Y., Irifune, T., Katsura, T., 2017b. Phase relations in the system MgSiO<sub>3</sub>-Al<sub>2</sub>O<sub>3</sub> up to 2300 K at lower-mantle pressures. *J. Geophys. Res.* 10, 7775–7788.
- McCammon, C.A., 1997. Perovskite as a possible sink for ferric iron in the lower mantle. *Nature* 387, 694–696.

- Murakami, M., Hirose, K., Yurimoto, H., Nakashima, S., Takafuji, N., 2002. Water in Earth's lower mantle. *Science* 295, 1885–1887.
- Navrotsky, A., 1999. A lesson from ceramics. *Science* 284, 1788–1789.
- Navrotsky, A., Schoenitz, M., Kojitani, H., Xu, H., Zhang, J., Weidner, D.J., Jeanloz, R., 2003. Aluminum in magnesium silicate perovskite: formation, structure, and energetics of magnesium-rich defect solid solutions. *J. Geophys. Res.* 108, 2330.
- Pamato, M., Myhill, R., Ballaran, T., Frost, D., Heidelbach, F., Miyajima, N., 2015. Lower-mantle water reservoir implied by the extreme stability of a hydrous aluminosilicate. *Nat. Geosci.* 8 (1), 75–79.
- Panero, W.R., Benedetti, L.R., Jeanloz, R., 2003. Transport of water into lower mantle: role of stishovite. *J. Geophys. Res.* 108.
- Panero, W.R., Pigott, J.S., Reaman, D.M., Kabbes, J.E., Liu, Z., 2015. Dry (Mg, Fe)SiO<sub>3</sub> perovskite in the Earth's lower mantle. *J. Geophys. Res.* 120 (2), 894–908.
- Pawley, A., McMillan, P.F., Holloway, J.R., 1993. Hydrogen in stishovite, with implications for mantle water content. *Science* 261, 1024–1026.
- Shcheka, S.S., Keppler, H., 2012. The origin of the terrestrial noble-gas signature. *Nature* 490, 531–534.
- Tschauner, O., Ma, C., Beckett, J.R., Precher, C., Prakapenka, V.R., Rossman, G.R., 2014. Discovery of bridgmanite, the most abundant mineral in Earth, in a shocked meteorite. *Science* 346, 1100–1101.
- Walter, M., Kubo, A., Yoshino, T., Brodholt, J., Koga, K.T., Ohishi, Y., 2004. Phase relations and equation-of-state of aluminous Mg-silicate perovskite and implications for Earth's lower mantle. *Earth Planet. Sci. Lett.* 222, 501–516.
- Walter, M., Tronnes, R.G., Armstrong, L.S., Lord, O., Caldwell, W.A., Clark, A.M., 2006. Subsolidus phase relations and perovskite compressibility in the system MgO–AlO<sub>1.5</sub>–SiO<sub>2</sub> with implications for Earth's lower mantle. *Earth Planet. Sci. Lett.* 248, 77–89.
- Zhang, J., Weidner, D.J., 1999. Thermal equation of state of aluminum enriched silicate perovskite. *Science* 284, 782–784.